Acta Biomaterialia xxx (2013) xxx–xxx

Contents lists available at SciVerse ScienceDirect

Acta Biomaterialia

journal homepage: www.elsevier.com/locate/actabiomat

Single-step electrochemical deposition of antimicrobial orthopaedic coatings based on a bioactive glass/chitosan/nano-silver composite system

F. Pishbin [a], V. Mouriño [b,c], J.B. Gilchrist [a,d], D.W. McComb [g], S. Kreppel [a,e], V. Salih [f], M.P. Ryan [a,d,*], A.R. Boccaccini [a,e,*]

[a] Department of Materials, Imperial College London, Prince Consort Road, London SW7 2BP, UK
[b] Department of Pharmaceutical Technology, Faculty of Pharmacy and Biochemistry, University of Buenos Aires, 956 Junín St., Buenos Aires CP1113, Argentina
[c] National Science Research Council (CONICET), Buenos Aires, Argentina
[d] London Centre for Nanotechnology, Imperial College London, Prince Consort Road, London SW7 2BP, UK
[e] Institute of Biomaterials, Department of Materials Science and Engineering, University of Erlangen-Nuremberg, 91058 Erlangen, Germany
[f] Division of Biomaterials & Tissue Engineering, Eastman Dental Institute, University College London, London WC1X 8LD, UK
[g] Department of Materials Science and Engineering, The Ohio State University, Columbus, Ohio 43210, USA

ARTICLE INFO

Article history:
Received 25 November 2012
Received in revised form 12 February 2013
Accepted 11 March 2013
Available online xxxx

Keywords:
Composite coatings
Bioglass®
Chitosan
Silver nanoparticles
Electrophoretic deposition

ABSTRACT

Composite orthopaedic coatings with antibacterial capability containing chitosan, Bioglass® particles (9.8 μm) and silver nanoparticles (Ag-np) were fabricated using a single-step electrophoretic deposition (EPD) technique, and their structural and preliminary in vitro bactericidal and cellular properties were investigated. Stainless steel 316 was used as a standard metallic orthopaedic substrate. The coatings were compared with EPD coatings of chitosan and chitosan/Bioglass®. The ability of chitosan as both a complexing and stabilizing agent was utilized to form uniformly deposited Ag-np. Due to the presence of Bioglass® particles, the coatings were bioactive in terms of forming carbonated hydroxyapatite in simulated body fluid (SBF). Less than 7 wt.% of the incorporated silver was released over the course of 28 days in SBF and the possibility of manipulating the release rate by varying the deposition order of coating layers was shown. The low released concentration of Ag ions (<2.5 ppm) was efficiently antibacterial against *Staphyloccocus aureus* up to 10 days. Although chitosan and chitosan/Bioglass® coating supported proliferation of MG-63 osteoblast-like cells up to 7 days of culture, chitosan/Bioglass®/Ag-np coatings containing 342 μg of Ag-np showed cytotoxic effects. This was attributed to the relatively high concentration of Ag-np incorporated in the coatings.

1. Introduction

In spite of notable advances in clinical methods, implanting a metallic orthopaedic device with long-term survivability still represents a major challenge for orthopaedic surgeons [1]. In terms of improving the surface functionality of metallic implants [2], bioactive glass coatings have demonstrated promising functionality [3]. These coatings can be further improved by combining bioactive glass with an organic polymer. Addition of a polymer phase to an inorganic coating may mechanically strengthen the glass or ceramic coating structure [4], eliminate high-temperature processing [5], control the ionic release rate of the bioactive ceramic [6], and perhaps more importantly, can provide a platform for incorporation and release of biomolecules and drugs which often require room-temperature processing [7].

Chitosan, a natural polysaccharide, is a well-known candidate for such a composite system. It is a linear, cationic polymer consisting of β (1 → 4)-glucosamine and *N*-acetyl-D-glucosamine and is obtained from *N*-deacetylation of chitin. Notable features of this biopolymer are susceptibility to enzymatic degradation, accelerated angiogenesis, little fibrous encapsulation, ability to link to and deliver growth factors, and improved cellular adhesion [8,9]. Moreover, chitosan has excellent film-forming property and has been the focus of many coating systems for biofunctionalization of metallic implants [10–13].

Implantation of an orthopaedic device in the body is always associated with a risk of microbial infection which is more severe

* Corresponding authors. Addresses: Institute of Biomaterials, Department of Materials Science and Engineering, University of Erlangen-Nuremberg, 91058 Erlangen, Germany. Tel.: +49 9131 85 28601 (A.R. Boccaccini), Department of Materials, Imperial College London, Prince Consort Road, London SW7 2BP, UK (M.P. Ryan).
E-mail addresses: m.p.ryan@imperial.ac.uk (M.P. Ryan), aldo.boccaccini@ww.uni-erlangen.de (A.R. Boccaccini).

1742-7061/$ - see front matter © 2013 Acta Materialia Inc. Published by Elsevier Ltd. All rights reserved.
http://dx.doi.org/10.1016/j.actbio.2013.03.006

in open-fractured bones and joint revision surgeries [14]. More importantly, formation of bacterial biofilms on the implant presents additional complications, as these are extremely resistant to both the immune system and antibiotics [15]. Unfortunately systemic drug administration in such clinical condition is not sufficiently effective due to impaired blood circulation at the injury site and low local concentration of drug. Therefore local delivery of drugs and biomolecules can be an effective approach to treat infections with high local concentrations of drug, with long-term controlled release and without the risk of systemic toxicity or formation of biofilms [16]. Various organic and inorganic coating systems with therapeutic capability have been explored [17].

As increased antibiotic resistance is a major medical concern, silver—an agent which has not developed bacterial resistance—is emerging as an antibacterial component with high potential. It works against a broad range of gram-positive (e.g. *Staphylococcus aureus* and *Staphylococcus epidermidis*) and gram-negative (e.g. *Escherichia coli*, *Pseudomonas aeruginosa*) bacteria [2]. Silver exhibits a bactericidal effect at very low concentrations without toxicity to human cells [18]. It has been incorporated in a variety of organic [19,20] and inorganic [21–24] coatings. More interestingly, it has been shown that silver nanoparticles have larger surface area contacting bacterial cells and hence have a higher level of interaction and faster release rate [25]. Films of chitosan-nano-silver/heparin produced via layer-by-layer deposition have shown antibacterial effects to *E. coli* without cytotoxicity to osteoblast cells [26]. Ag-doped HA/PEEK composite coatings cold-sprayed on glass slides have inhibited the growth of bacteria [27]. In another study by Roy et al. [28], significant reduction in *S. aureus* and *P. aeruginosa* colonies were observed on Ag-tricalcium phosphate-coated Ti surfaces.

Among different techniques exploited for composite orthopaedic coatings, electrophoretic deposition (EPD) is particularly attractive because it can be utilized to produce uniform coatings with controlled properties on complex-shaped and porous structures, at ambient temperature and without the need for expensive processing equipment [29]. Co-deposition of polymers and ceramics is also another interesting feature of EPD [5,29,30]. In EPD, surface-charged particles in suspension move toward an oppositely charged electrode (i.e. the substrate) under an applied electrical field and form a coating. Many different composite biomaterial coatings have been fabricated by EPD [30]. Recently we have investigated the influence of EPD parameters on co-deposition of Bioglass® particles and chitosan from aqueous medium [5]. Pang et al. [31] have applied EPD to co-deposit multilayers of composite chitosan/silver/hydroxyapatite (HAp) nanoparticles. They have reported formation of amorphous Ag–chitosan complexes in their coatings and have controlled the release kinetics of ionic silver from these coatings by application of an additional chitosan film.

We have previously studied in detail the effect of EPD parameters on deposition of chitosan coatings [10], Bioglass® coatings [32] and chitosan/Bioglass® composite coatings [5]. The next step is addition of an antibacterial function to the chitosan/Bioglass® composite coatings and we are keen to demonstrate the potential of EPD as a single-step platform for obtaining such a coating. Hence, the goal of this research is the single-step fabrication and characterization of multifunctional resorbable chitosan/bioactive glass composite coatings containing silver in the form of Ag nanoparticles (Ag-np). In this work, co-deposition of the chitosan/bioactive glass composite coating in addition to simultaneous *in situ* formation and deposition of Ag-np as antibacterial agent has been demonstrated for the first time. More importantly, considering the environmental concerns associated with free nanoparticles, the benefit of the developed technique is the absence of loose nanoparticles in all steps. The microstructural aspects of the coatings have been examined by different techniques. A preliminary in vitro cellular and antibacterial study to characterize the behaviour of these films was conducted. This investigation can contribute to a better understanding of the interaction between the biological environment and these novel materials intended for orthopaedic and bone engineering applications.

2. Experimental procedures

2.1. Materials

45S5 Bioglass® powder with nominal composition $45SiO_2$–$24.5Na_2O$–$24.5CaO$–$6P_2O_5$ (wt.%) was kindly supplied by Dr. I. Thompson (Kings College London, UK). The particle size was in the range 1.6 and 26.7 μm with a median particle size of 9.8 μm. Medium molecular weight chitosan (MW = 80 kDa) with a degree of deacetylation of about 85% and acetic acid (>98%) were purchased from Sigma–Aldrich and 0.05 M silver nitrate solution (AVS TITRINORM) from VWR was used. The following reagents from Sigma–Aldrich were used to prepare simulated body fluid (SBF) solution [33]: NaCl, $NaHCO_3$, KCl, $K_2HPO_4{\cdot}3H_2O$, $MgCl_2{\cdot}6H_2O$, $CaCl_2$, Na_2SO_4, Tris-hydroxymethyl aminomethane and HCl (1.0 M).

2.2. Electrophoretic deposition

Dilute solutions of chitosan (0.5 mg ml^{-1}) in 1 vol.% acetic acid in deionized water were prepared by magnetic stirring at room temperature for 24 h. Suspensions containing Bioglass® were prepared by dispersing the particles in the chitosan solutions via magnetic stirring and sonication (USC 300 sonicator, VWR International, Malaysia) for periods of 600 s each. For coatings containing Ag-np, silver nitrate solution was added to the prepared suspensions with a final concentration of 1 mM. The pH of the suspensions was measured by using Jenway 3510 pH meter (Essex, UK).

AISI 316L stainless steel is among the most commonly used metals for orthopaedic implant applications [34]. Thus, for electrophoretic deposition, AISI 316L (Advent Research Materials Ltd., Oxford, UK) foils (20 mm × 10 mm × 0.2 mm) were utilized as deposition substrate. It is pertinent to point out that for similar substrate surface conditions, as long as the substrate is electrically conductive, the EPD rate is independent of the substrate material [29]. Therefore, the methodology applied here is extendable to other conductive implant substrate materials such as Ti alloys. Substrates were washed with acetone and dried prior to deposition. A gold counter-electrode was used in the EPD cell. Experiments were performed at 21 ± 2 °C. The distance between the electrodes was kept constant at 1.5 cm and the suspensions were gently stirred during deposition by a magnetic stirrer. The constant electric voltage was applied by a Thurlby Thandar Instruments (TTi) EL561 power supply (Huntingdon, UK). Four different coatings were deposited. The EPD experimental condition for each coating is outlined in Table 1. After deposition, the cathodic films were gently rinsed with deionized water, dried and stored in a desiccator for further characterization.

2.3. Characterization of coatings

2.3.1. Microstructural characterization

High-resolution scanning electron microscopy (SEM; LEO Gemini 1525) was used to study the microstructural features. The samples were coated with chromium using an Emitech K575X sputter coater (Emitech Ltd., UK) beforehand to avoid any charging artefacts during imaging. The LEO Gemini 1525 microscope was equipped for energy-dispersive X-ray spectrometry

Please cite this article in press as: Pishbin F et al. Single-step electrochemical deposition of antimicrobial orthopaedic coatings based on a bioactive glass/chitosan/nano-silver composite system. Acta Biomater (2013), http://dx.doi.org/10.1016/j.actbio.2013.03.006

Table 1
EPD parameters for deposition of biomedical coatings from 0.5 mg ml^{-1} chitosan solutions.

Coating type	Coating name	Bioglass® (mg ml^{-1})	Silver nitrate (mM)	Voltage (V)	Time (s)
Chitosan	CS	0	0	10	800
Chitosan/Bioglass®	CS/BG	5	0	10	400
Chitosan/Ag-np	CS/Ag	0	1	10	300
Chitosan/Bioglass®/Ag-np	CS/BG/Ag	3	1	15	400

(EDS; INCA, Oxford Instruments) for qualitative elemental analysis of the coatings.

The crystalline state of the material was checked with X-ray diffraction (XRD) analysis using a PANalytical X'Pert Pro MPD instrument with Cu-K_α radiation at 40 KV and 40 mA, applying a step size of 0.04° for the 2θ range 5°–80° and with a count rate of 50 s per step.

Fourier transform infrared spectroscopy (FTIR) was performed in transmission mode using a Perkin–Elmer Multiscope spectrometer in the mid-IR region (5000–400 cm^{-1}). For FTIR analysis, the coatings were removed from the substrates, mixed and ground with potassium bromide (KBr) at a weight ratio of 1:100 and pressed into pellets.

In order to estimate the composition of the coatings, they were removed from the substrates and thermogravimetric analysis (TGA) and differential scanning calorimetry (DSC) was performed in air using a simultaneous thermal analyser (Netzsch STA 449 C, Germany). A heating rate of 10 °C min^{-1} was utilized and three samples were tested per coating condition.

2.3.2. Transmission electron microscopy

To identify the location and morphology of any deposited silver components incorporated into the coatings, the EPD films were examined by transmission electron microscopy (TEM). Thin cross-sections of CS/Ag and CS/BG/Ag samples were prepared with a focused ion beam (FIB) dual beam system (FEI™ helios™ NanoLab™) using the *in situ* lift-out technique [35]. After coating with a chromium layer to provide a conductive surface and a platinum strap to protect surface features, the selected area of the coating was milled using 30 kV accelerated Ga^+ ions to create a lamella. The extracted lamella was attached to a copper TEM grid and thinned down to electron transparency with the Ga^+ beam at successively lower accelerating voltages, with the final voltage set at 2 kV and a beam-defining aperture corresponding to a 3.2 pA beam current. The microstructure was examined using JEOL 2010F and Philips CM200 transmission electron microscopes, both operated at 200 kV in bright-field mode, and selected-area electron diffraction (SAED) patterns were obtained to confirm the crystallinity of Ag-np.

2.3.3. Acellular in vitro study by immersion in simulated body fluid

To investigate the level of acellular in vitro bioactivity of coatings in terms of HAp formation, the SBF test proposed by Kokubo et al. [33] was performed. Coated samples (10 mm × 10 mm × 0.2 mm) were immersed in 30 ml SBF and were then incubated at 37 °C for 5, 7, 14, 21 and 28 days. At each time point the sample was removed from SBF, rinsed with ion-exchanged and distilled water, left to dry in air and then stored in a desiccator. The formation of HAp was examined with SEM/EDX, XRD and FTIR after SBF immersion. For comparison, samples before immersion in SBF were also characterized.

2.3.4. Silver release study

The concentration of silver ions in the EPD suspension before and after deposition was estimated by inductively coupled plasma optical emission spectroscopy (ICP-OES; Thermo Scientific, ICP 6000 series). Furthermore, the release of Ag ions in SBF solution was investigated by incubating samples of Ch/BG/Ag-np in 10 ml SBF at 37 °C. At specific time points (3, 6 h, 12 h, 1, 3, 5, 7, 14, 21 and 28 days), 2 ml aliquots were removed from samples and refreshed with fresh SBF. For ICP-OES studies, the collected samples were further diluted with deionized water. To investigate the possibility of controlling the release of Ag ions, a bilayer coating consisting of an initial layer of CS/Ag covered by a second layer of chitosan/Bioglass® composite (EPD parameters: 0.5 mg ml^{-1} chitosan, 3 mg ml^{-1} Bioglass®, 15 V, 400 s) was electrophoretically deposited. The release of Ag ion in SBF from this bilayer film was compared with the release from the monolayer CS/BG/Ag film.

2.4. Biocompatibility studies

2.4.1. Microbiological study

The effect of the incorporation of Ag-np in coatings on the viable counts of *S. aureus* (ATCC 25923) was investigated by conducting agar disk diffusion tests on CS, CS/BG and CS/BG/Ag-np samples with 316 SS and PBS as controls. Prior to the study, coatings were sterilized by UV treatment for 45 min each side. Five samples of each series (10 mm × 10 mm × 0.2 mm) were immersed at 37 °C in PBS (5 ml) at pH 7.4 for 10 days. At predetermined time intervals (1, 2, 3, 5, 7 and 10 days) aliquots (5 μl) of each series were removed and applied to paper discs and placed on the surface of Mueller–Hinton agar plates seeded with *S. aureus* through a modification of the agar disk diffusion method of CLSI (CLSI 2010). After each aliquot was taken, the remaining volume was replaced with fresh PBS to mimic physiological clearance. Approximately 107 colony-forming units (CFU) of *S. aureus* were inoculated on Mueller–Hinton agar plates. After 24 h of incubation, the zones of inhibition were measured. Bacteria were streaked on Trypticase soy agar (Difco, USA) from −70 °C stocks. Overnight agar cultures were transferred to tryptic soy broth (Difco, USA) and incubated at 37 °C statically for 48 h. After centrifugation (8000*g*, 4 °C, 10 min), bacteria were resuspended to 1.5 × 10^8 CFU ml^{-1}.

2.4.2. In vitro cellular study

MG-63 osteoblast, a human osteosarcoma cell line, was used to assess the in vitro cytocompatibility of CS, CS/BG, CS/BG/Ag-np coatings, and 316 SS uncoated substrate and tissue culture plastic (TCP) were used as controls. Cells were cultured in low glucose (1 g l^{-1}), L-glutamine containing Dulbecco's Modified Eagle's Medium (DMEM)), supplemented with 10% (v/v) fetal bovine serum (FBS) and 1% (v/v) antibiotic (penicillin/streptomycin) solution (all from PAA, Coelbe, Germany) (which will be referred to hereafter as "complete medium"). Prior to testing, the samples (10 mm × 10 mm × 0.2 mm) were UV-sterilized for 45 min each side.

80–85% confluent cultures were harvested for experiments with a solution of 0.05%/0.002% Trypsin/EDTA in Ca^{2+}/Mg^{2+}-free PBS (PAA) and pelleted by centrifugation at 1000 rpm for 5 min. Cell counting was done by trypan blue dye and haemocytometry. The test samples were seeded at a density of 20,000 cells cm^{-2} and were incubated in 1 ml complete medium at 37 °C in a humidified atmosphere (5% CO_2 in 95% air). After an overnight period, samples were transferred to a new well plate and replenished with fresh medium. The cells were then allowed to grow on the coatings for

Please cite this article in press as: Pishbin F et al. Single-step electrochemical deposition of antimicrobial orthopaedic coatings based on a bioactive glass/chitosan/nano-silver composite system. Acta Biomater (2013), http://dx.doi.org/10.1016/j.actbio.2013.03.006

up to 7 days, with the medium changed every 2 days. At specific time intervals, the cell proliferation measurement was carried out using the alamarBlue® assay (AbD Serotec, Oxford, UK). At the end of each time point, 100 μl of the culture medium was replaced with alamarBlue® indicator dye and incubated for 4 h. Sample aliquots of 100 μl were then taken and their fluorescence measured at excitation and emission wavelengths of 530 and 590 nm, respectively (Thermo Labsystems Fluoroskan Ascent FL, Waltham, MA, USA). The number of viable cells was estimated by interpolating fluorescence readings from a six-point standard alamarBlue® curve. The standard curve ($R^2 = 0.9902$) was obtained by 1:2 serial dilution of the initial 1×10^5 cell number. The resultant number of cells for each coating was normalized against the number of cells on TCP at day 1 culture and was reported as a percentage. The results represent the mean ± standard deviation (SD) of two individual experiments each performed in quadruplicate.

2.5. Data analysis

The experiments were performed in multiple numbers per series (four or five samples) and the results were reported as mean ± SD. One-way analysis of variance (ANOVA) with $P < 0.05$ as the level of significance was utilized for statistical analysis, and the Tukey test was used for comparison of means.

3. Results

3.1. Characterization of coatings

3.1.1. Microstructural characterization

SEM analyses of different coatings are shown in Fig. 1. Although CS coatings have a smooth surface morphology (Fig. 1a, cracks are due to damage by the accelerated electrons), CS/Ag films (Fig. 1b) contain particulate structures embedded in the chitosan matrix. On the other hand, the microstructures of both CS/BG and CS/BG/Ag films (Fig. 1c and d, respectively) consist of a chitosan polymeric matrix with micron-sized Bioglass® particles uniformly distributed in it. Higher-magnification images of CS/BG/Ag coating show areas in which clusters of nanoparticulate material are attached to each other by chitosan polymer. It is anticipated that these are Ag-np.

EDX analyses of the deposited films (Fig. 2b and d) confirm the presence of silver in both CS/Ag and CS/BG/Ag coatings in comparison to CS coatings (Fig. 2a). The peaks of Si, Na, Ca and P in the EDX spectrum (Fig. 2b and d) correspond to the Bioglass® component.

According to the XRD patterns (Fig. 3), CS film exhibits a broad peak at ~20° corresponding to the semicrystalline nature of chitosan [36]. The composite CS/BG coating has an amorphous structure displaying very broad peak at ~30°, which corresponds to the presence of Bioglass®. Silver nitrate addition to the EPD suspension has

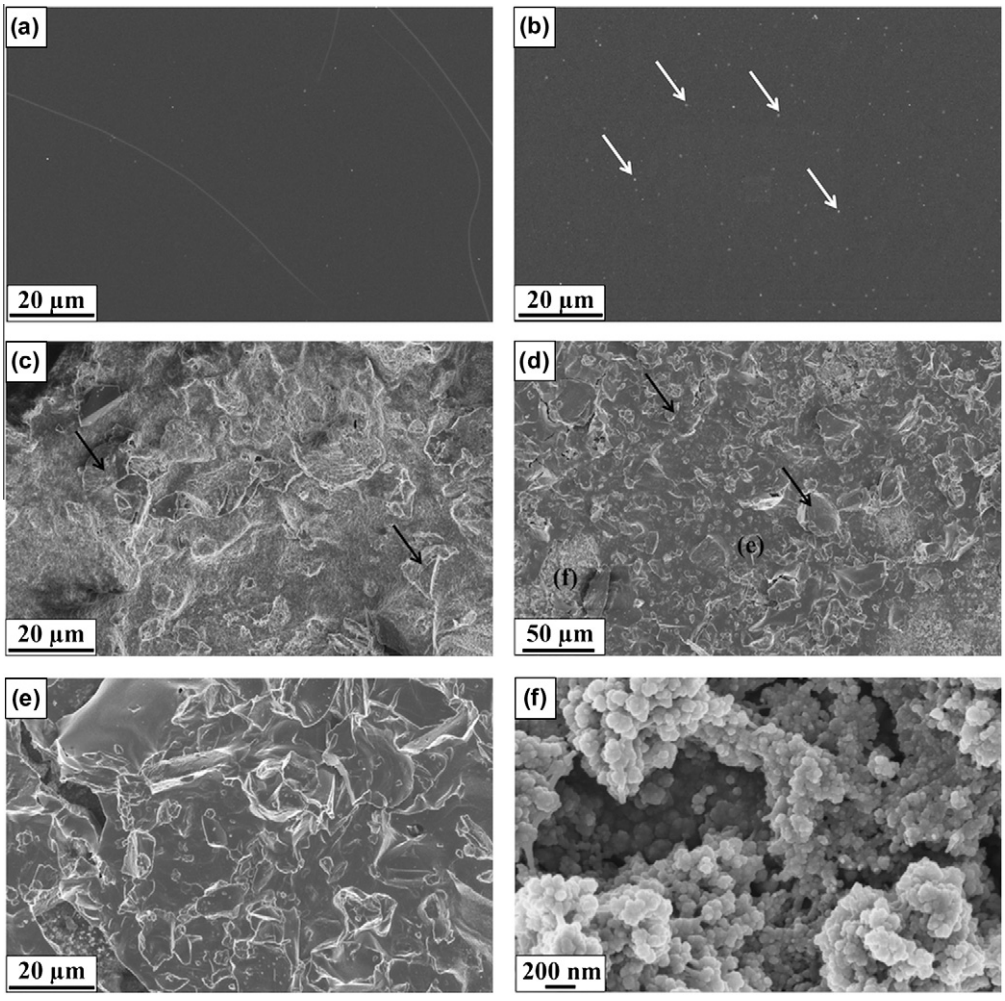

Fig. 1. SEM images of CS (a); CS/Ag (b); CS/BG (c); CS/BG/Ag (d) coatings; higher-magnification images of Bioglass® microparticles containing (e) and silver nanoparticles containing (f) locations in CS/BG/Ag coating. The silver nanoparticles (white arrows) and Bioglass® microparticles (black arrows) are indicated.

Please cite this article in press as: Pishbin F et al. Single-step electrochemical deposition of antimicrobial orthopaedic coatings based on a bioactive glass/chitosan/nano-silver composite system. Acta Biomater (2013), http://dx.doi.org/10.1016/j.actbio.2013.03.006

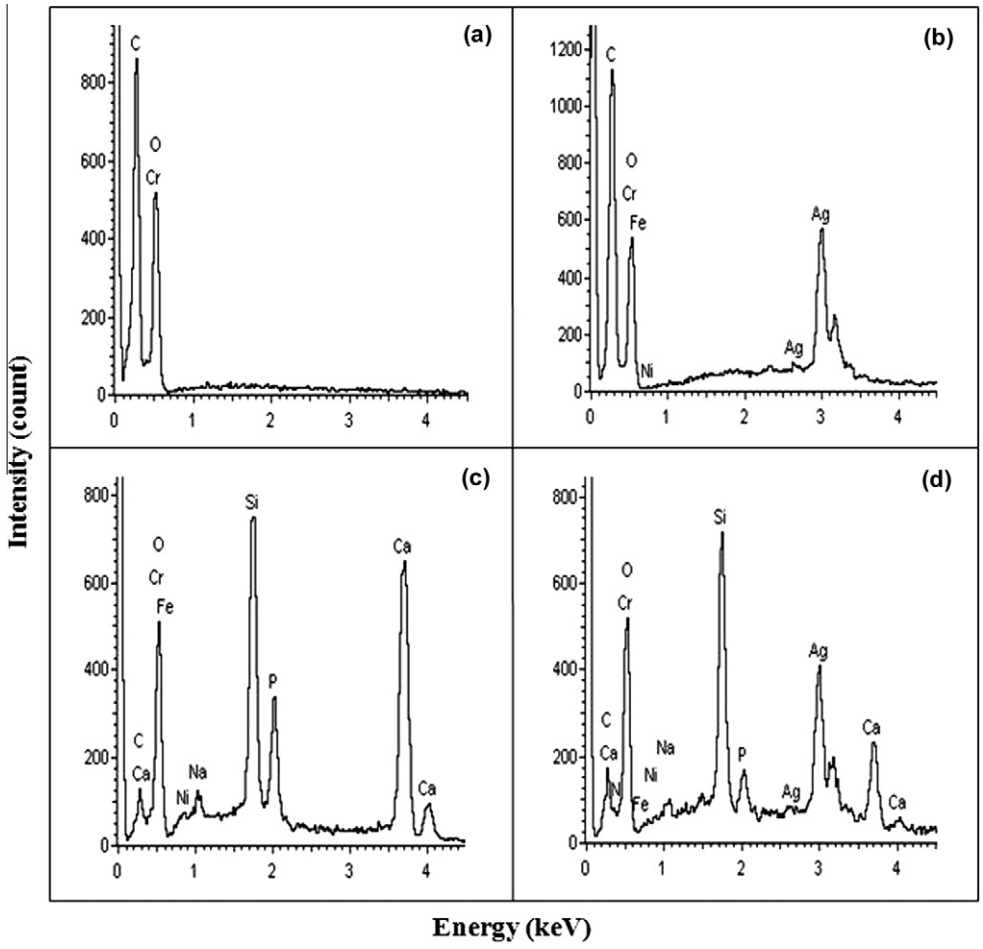

Fig. 2. EDX spectra of CS (a), CS/Ag (b), CS/BG (c) and CS/BG/AG (d) coatings.

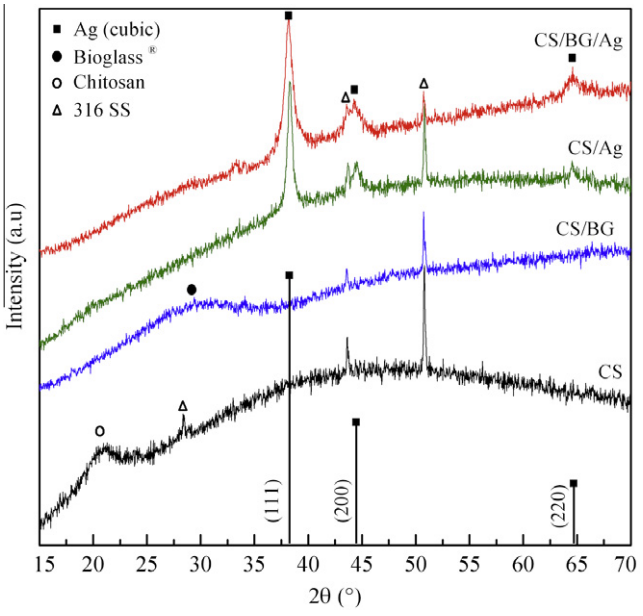

Fig. 3. XRD patterns of CS, CS/Ag, CS/BG and CS/BG/Ag coatings and the peaks corresponding to different phases (316 SS peaks shown are from the metallic substrate).

resulted in deposition of a new crystalline phase, the pattern of which matches that of silver metal with cubic crystalline structure.

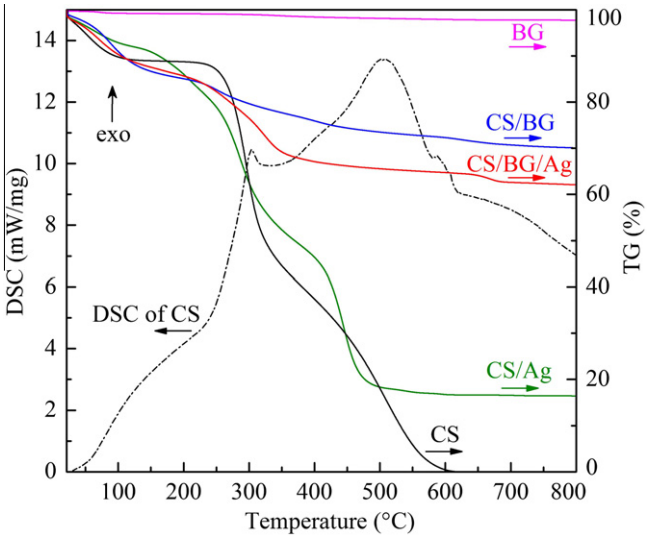

Fig. 4. TGA curves comparing Bioglass® powder, CS, CS/Ag, CS/BG and CS/BG/Ag coatings showing the weight loss due to water evaporation and burning out of chitosan. (Three samples were tested per coating condition).

Therefore it is concluded that the deposited nanoparticles in the films are Ag-np. It should be noted that the high and very broad background observed in all XRD plots is due to substrate iron fluorescence.

Please cite this article in press as: Pishbin F et al. Single-step electrochemical deposition of antimicrobial orthopaedic coatings based on a bioactive glass/chitosan/nano-silver composite system. Acta Biomater (2013), http://dx.doi.org/10.1016/j.actbio.2013.03.006

Simultaneous thermal analyses (STA) of the coatings are depicted in Fig. 4. As the TGA curves show, the coatings undergo several stages of weight loss with increasing temperature. Below 100 °C the moisture in the coatings evaporates. Following that, the two-stage burning out of chitosan polymer occurs at temperatures of 220–350 °C and 380–600 °C. The DSC data of CS coating has two exothermic peaks at ~300 and ~500 °C corresponding to these two stages [37]. The TGA curve of the as-received Bioglass® powder (BG) shows about 3% weight loss due to loss of moisture and hydroxyl groups. The decrease in weight loss from CS to CS/Ag and CS/Ag/BG, respectively, evidences incorporation of silver and Bioglass® particles in the films. The lower amount of weight loss in the CS/BG deposit compared to CS/BG/Ag coating can be due to the higher concentration of Bioglass® particles in the EPD suspension of the former deposit. Due to lower amount of chitosan in the CS/BG and CS/BG/Ag films, their TGA curves do not display the second stage of chitosan burning out as clearly as in CS and CS/Ag coatings. The amount of particles incorporated in composite films was determined to be 70.03 ± 0.05 wt.% Bioglass® in CS/BG, 16.2 ± 0.6 wt.% silver in CS/Ag and 63.79 ± 0.08 wt.% Bioglass® + silver in CS/BG/Ag.

3.1.2. Transmission electron microscopy

TEM imaging revealed the presence of nanoparticles at the interface between coatings and substrate in the CS/Ag and CS/BG/Ag films (Fig. 5). In CS/Ag coatings, 50–80 nm nanoparticles are covered with a layer of deposited chitosan (Fig. 5a). On the other hand a thicker layer of finer-sized Ag-np (<50 nm) infiltrated with chitosan polymer is observed in the CS/BG/Ag coatings (Fig. 5b). SAED of these TEM cross-sections demonstrates the polycrystalline diffraction pattern of silver in addition to the diffraction pattern from the 316 SS substrate. The interplanar spacings of 0.23, 0.21, 0.15 and 0.13 nm, correspond to the (111), (200), (220) and (311) planes of face-centred-cubic silver, respectively. It is noteworthy that due to larger scale of bioactive glass particles compared to Ag-np, the CS/BG/Ag TEM cross-section was intentionally prepared from a small area that did not contain microparticles of Bioglass® (such as (f) area in Fig. 1d) and therefore only chitosan and Ag-np are seen in the TEM image.

3.1.3. Acellular in vitro study in SBF

As Fig. 6 demonstrates, after 28 days of immersion in SBF, no deposition of HAp was detected by SEM/EDX of CS film. The chlorine detected from EDX of CS coatings has been incorporated in the polymer from the SBF solution. The XRD of SBF-treated CS coating (Fig. 7) confirms the amorphous structure of this CS film. On the other hand, a new nanostructured phase has formed on the surfaces of both CS/BG and CS/BG/Ag coatings after as little as 5 days of SBF immersion. Comparison of the EDX spectra of these composite films before (Fig. 2c and d) and after (Fig. 6b and c) SBF immersion shows that the new phase has an increased amount of Ca and P atoms, contains a small amount of Mg atoms and no Si and Na peaks can be found. XRD analyses of these coatings (Fig. 7) thus confirm that the newly formed phase on composite coatings is HAp and its crystallinity increases with SBF immersion time. A closer look at the HAp formed shows that the morphology of this phase on CS/BG is different from the one formed on CS/BG/Ag (Fig. 6b and c, insets). While the HAp nanocrystals deposited on the former are rod-shaped, the ones grown on the latter have a plate-like morphology. Fig. 6c displays an area of Ag-np containing chitosan surrounded by parts in which HAp crystals have grown on the composite coating. The charging effects observed in the SEM image (Fig. 6b) is due to the porous nature of the newly formed HAp layer.

Formation of HAp in the Ag-np containing composite coatings has been also elucidated by comparing FTIR spectra before and

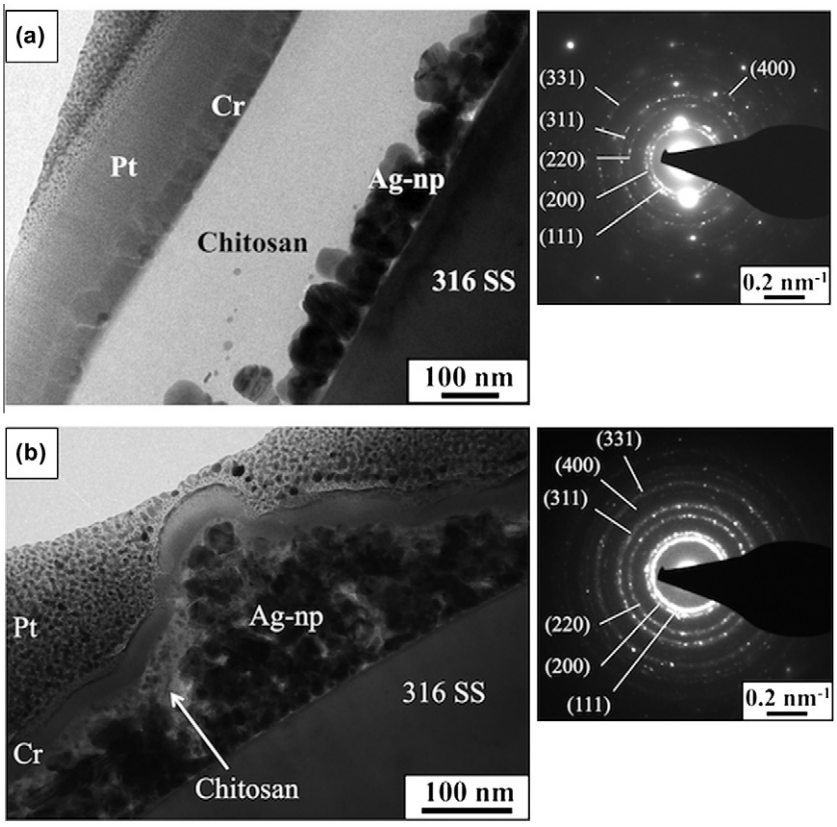

Fig. 5. TEM cross-sections of CS/Ag (a) and CS/BG/Ag (b) films with their corresponding selected-area diffraction patterns (insets).

Please cite this article in press as: Pishbin F et al. Single-step electrochemical deposition of antimicrobial orthopaedic coatings based on a bioactive glass/chitosan/nano-silver composite system. Acta Biomater (2013), http://dx.doi.org/10.1016/j.actbio.2013.03.006

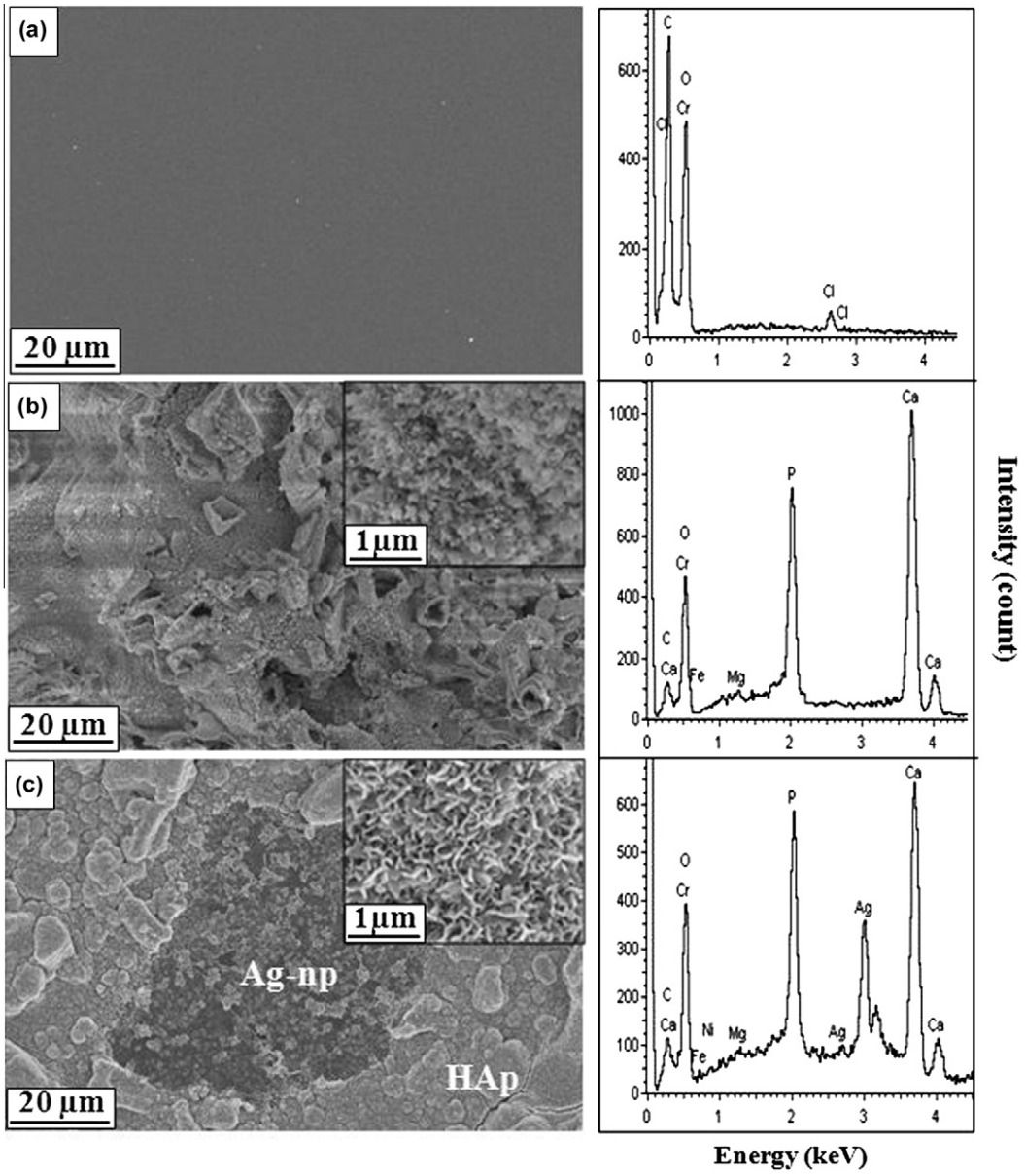

Fig. 6. SEM images and EDX analysis of coatings treated in SBF; CS after 28 days (a); CS/BG after 5 days (b); and CS/BG/Ag after 5 days (c). Insets: higher-magnification images of hydroxyapatite (HAp) phase.

after SBF immersion. In order to fully characterize the obtained coatings, the FTIR spectra of CS coating and pure Bioglass® were also studied. As shown in Fig. 8, the main bands of chitosan appear in various ranges. The broad band in the range 3750–3000 cm^{-1} is due to overlaying of several bands—the stretching vibration of OH groups from the carbohydrate ring and also adsorbed water (3500–3450 cm^{-1}) plus N–H stretching in amine and amide (~3300 cm^{-1}). This is followed by vibration bands of the C–H bond in $–CH_2$ (2930 cm^{-1}) and $–CH_3$ (2875 cm^{-1}). Moreover, $–CH_3$ symmetrical deformation and $–CH_2$ bending vibration occur at 1380 and 1420 cm^{-1}, respectively. The range of 1680–1480 cm^{-1} is attributed to two functional groups: vibration of carbonyl bond (C═O) in the amide group at 1660 cm^{-1} and vibration of the amine ($–NH_2$) group at 1580 cm^{-1}. N–H has a vibration band at 1318 cm^{-1}. Finally, the peak in the 1160–1000 cm^{-1} range is assigned to CO groups: 1150 cm^{-1} is due to asymmetric vibration of CO in the oxygen bridge and the bands near 1080–1025 cm^{-1} are from the CO of the ring COH, COC and CH_2OH [38].

Alternatively the main peaks in the spectrum of pure Bioglass® are attributed to Si–O–Si bending vibration (509 cm^{-1}) and stretching vibration (950 and 1050 cm^{-1}; the dual peak is indicative of the presence of network modifiers such as Na and Ca in the structure of glass) [39]. The broad peak at 3500 cm^{-1} and the one at 1480 cm^{-1}, respectively, are due to hydroxyl and carbonate groups adsorbed from the atmosphere. In addition, the dual peak at about 2350 cm^{-1} is due to atmospheric CO_2.

The CS/BG/Ag composite FTIR spectrum (Fig. 8) indicates the presence of peaks associated with both chitosan and Bioglass®. There are slight changes in the position and intensity of the glass and polymer peaks, which are indicated by arrows. Shifting of glass Si–O–Si bending vibration to lower wavenumber and change in the intensity of IR transmission at carbonyl, amine, CH_2 and CH_3 bands can be indicative of interaction between chitosan, Bioglass® and silver ions (silver ion has later deposited as Ag-np).

After immersion in SBF and formation of biomimetic HAp phase, new peaks appear in the CS/BG/Ag spectrum (Fig. 8). The P–O

Please cite this article in press as: Pishbin F et al. Single-step electrochemical deposition of antimicrobial orthopaedic coatings based on a bioactive glass/chitosan/nano-silver composite system. Acta Biomater (2013), http://dx.doi.org/10.1016/j.actbio.2013.03.006

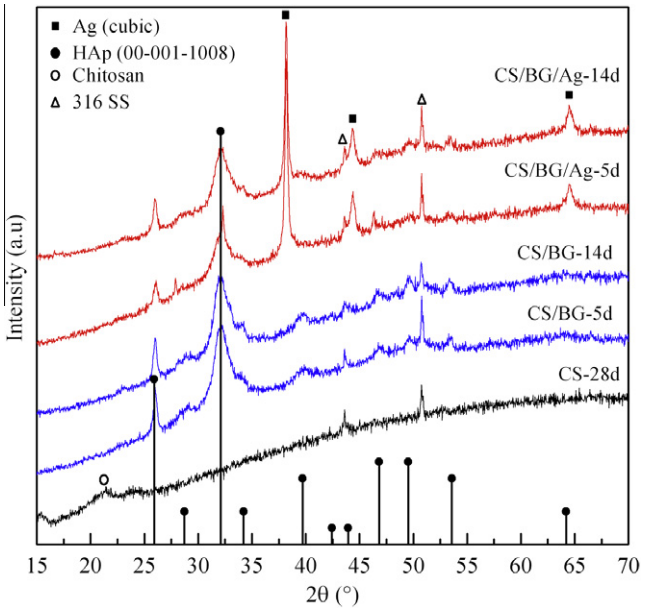

Fig. 7. XRD patterns of coatings treated in SBF; CS after 28 days (CS-28d); CS/BG after 5 and 14 days (CS/BG-5d, CS/BG-14d) and CS/BG/Ag after 5 and 14 days (CS/BG/Ag-5d, CS/BG/Ag-14d). The standard pattern for HAp is shown for comparison.

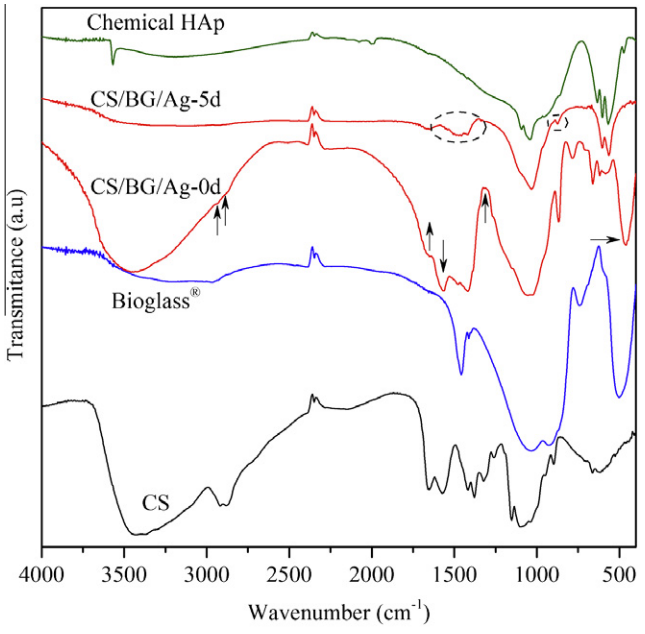

Fig. 8. FTIR spectra of CS, pure Bioglass®, CS/BG/Ag before and after 5 days SBF immersion (CS/BG/Ag-0d and CS/BG/Ag-5d) and chemical HAp as standard. Arrows show wavenumbers at which change in intensity or shifting has occurred. Dashed circled area indicates carbonate bands in biomimetic HAp.

bending vibration dual peak at 560 and 603 cm^{-1} and the P–O stretching peak at 1030 cm^{-1} are related to phosphate groups. Comparison of the spectrum of biomimetic HAp grown on the sample with that of chemical HAp reveals the presence of C–O out-of-plane bending (873 cm^{-1}) and C–O stretching (1530–1400 cm^{-1}) in the latter (dashed circled area displayed in Fig. 8). This fact confirms the biomimetically developed HAp (in SBF) is carbonated hydroxyapatite (HCAp).

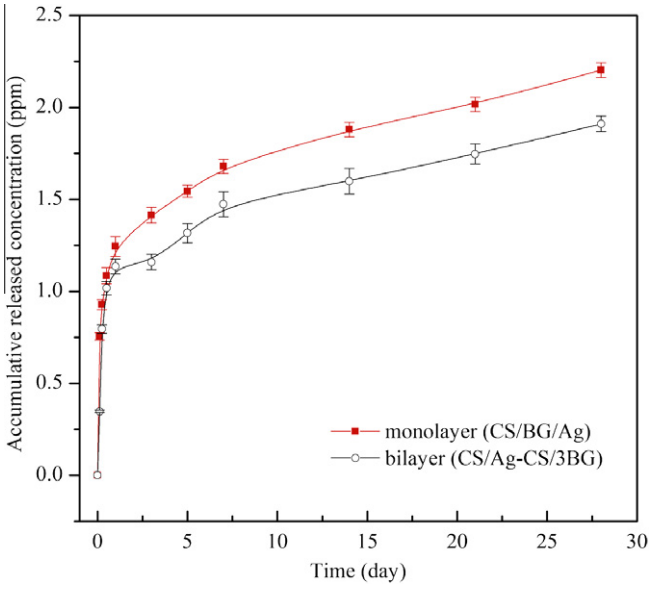

Fig. 9. Accumulative release of silver ion from monolayer (CS/BG/Ag) and bilayer (CS/Ag-CS/BG) coatings in SBF.

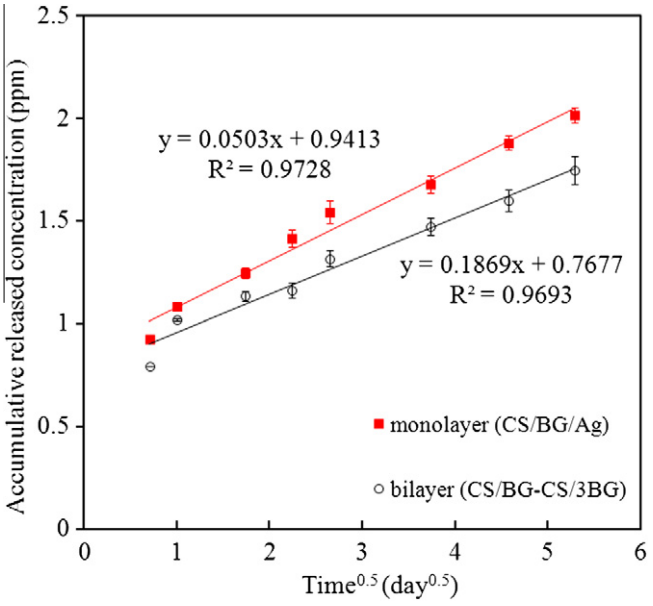

Fig. 10. Accumulative release of silver ion from monolayer (CS/BG/Ag) and bilayer (CS/Ag-CS/BG) coatings in SBF vs. square root of time.

3.1.4. Silver release study

The amount of silver incorporated in the CS/Ag and CS/BG/Ag coatings was estimated to be 362.5 ± 38.1 and 342 ± 24.8 μg. As Fig. 9 demonstrates, there is an initial burst release of Ag^+ followed by a reduced release rate. Additionally the monolayer releases more Ag^+ ions, suggesting the inhibitory effect of the outer layer (covering the inner CS/Ag layer) in the bilayer coating. This behaviour is more prominent after 24 h during which the formation of HAp is expected.

Another interesting aspect is the release behaviour after the initial burst release. As Fig. 10 shows, after about 6 h, the release of silver ions follows a linear trend with respect to the square root of immersion time in SBF solution. This can be indicative of a diffusion-controlled mechanism.

Please cite this article in press as: Pishbin F et al. Single-step electrochemical deposition of antimicrobial orthopaedic coatings based on a bioactive glass/chitosan/nano-silver composite system. Acta Biomater (2013), http://dx.doi.org/10.1016/j.actbio.2013.03.006

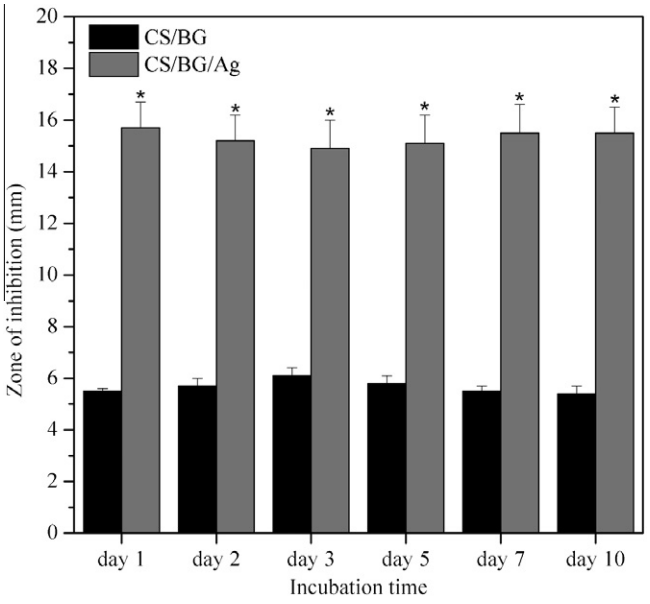

Fig. 11. Antimicrobial disk susceptibility test showing the relative diameters of zones of inhibition after different periods of immersion in PBS up to 10 days. The PBS control, 316SS and CS did not develop any zones of inhibition. The data represent mean ± SD of three individual experiments (*$P < 0.05$ CS/BG/Ag vs. CS/BG).

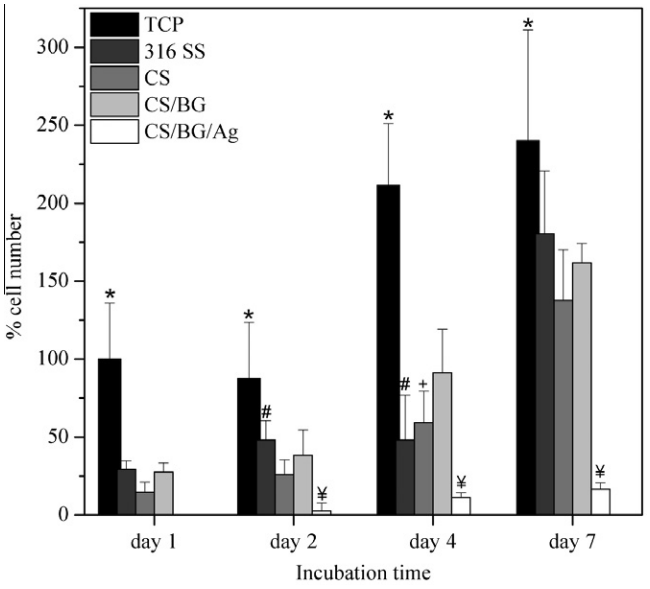

Fig. 12. Osteoblast-like human osteosarcoma cell line (MG-63) response to 316SS substrate, CS, CS/BG and CS/BG/Ag coatings measured by alamarBlue® assay up to 7 days culture. Tissue culture plastic (TCP) was used as control. Data represent mean ± SD of two individual experiments each performed in quadruplicate. ($P < 0.05$ at the same time period: * is for TCP vs. all other coatings; ¥ is for CS/BG/Ag vs. all other coatings; # is for marked bar vs. CS; + is for marked bar vs. CS/BG).

3.2. Biocompatibility studies

3.2.1. Microbiological study

The antimicrobial disk susceptibility test indicated that CS/BG/Ag coatings immersed for 10 days in PBS developed a zone of inhibition 15–16 mm in size. This result shows in vitro antibacterial activity of the released silver ions against *S. aureus*. Fig. 11 shows that according to the relative length of the zone of inhibition, CS/BG samples were also capable of inhibiting bacterial growth but at a significantly lower level (5.4–6 mm). This bacteriostatic effect of CS/BG can be related to the local increase in the pH during the degradation of Bioglass® [40]. The PBS control sample, 316SS and CS coatings did not develop a zone of inhibition against *S. aureus* growth.

3.2.2. In vitro cellular study

The cellular metabolic activity was measured by alamarBlue® assay, and based on that the cell number percentage was estimated. As Fig. 12 shows, CS, CS/BG and controls (316 SS and TCP) supported proliferation of MG-63 cells over the 7-day study period. At each time point, all coatings have significantly ($P < 0.05$) smaller cell numbers compared to TCP (positive control). After 7 days of culture, no significant difference was observed among 316 SS, CS and CS/BG samples. The proliferation of cells on all samples increased over the time of study. The important aspect to mention is the significantly ($P < 0.05$) lower percentage of cells on CS/BG/Ag samples compared to other coatings throughout the investigation. This behaviour might be indicative of incorporation of excessive levels of silver in the composite structure leading to cellular toxicity.

4. Discussion

The present results confirm the suitability of EPD as a processing method for the surface multifunctionalization of metallic substrates with potential orthopaedic application. The mechanisms of electrodeposition of chitosan and EPD of chitosan/Bioglass® composite have been previously studied [5,10]. Chitosan electrophoresis toward the negative electrode occurs due to protonation of its amino groups at the low solution pH and it deposits at the electrode due to water electrolysis and subsequent increase in the local pH (above chitosan pK_α) [10]. On the other hand, in the composite suspension, electrosteric and electrostatic effects provide improved Bioglass® microparticle dispersion and co-deposition of chitosan and glass particles, which results in the formation of a composite film [5]. This composite structure can improve the bioactivity and osseointegration of metallic orthopaedic devices. The novel aspect of the present work is the addition of antibacterial functionality to the above-mentioned bioactive composite coatings in a single-step EPD process. It involves *in situ* formation of Ag-np, and simultaneous incorporation of Ag-np into the structure of the composite. This approach eliminates the multiple steps required in conventional processing of such coatings, which involves preparing Ag-np; obtaining a stable suspension of them; and finally sequential deposition of particulate and polymeric components. An additional important advantage of *in situ* formation and encapsulation of Ag-np is that it avoids possible environmental hazards associated with loose nanoparticles.

Addition of silver nitrate to the EPD suspension of chitosan/Bioglass® facilitates formation of a chitosan–silver ion complex. Chitosan has been reported in the literature to be a metal-chelating polymer [26,41]. The lone pair of electrons on chitosan amine and hydroxyl groups provide preferable sites for absorption of electropositive transition metal ions of silver via electrostatic (ion–dipole) interactions [41]. Due to the high deacetylation degree of chitosan used in this work, mainly amine and hydroxyl groups are assumed to be involved, but the O of carbonyl group in the remaining acetylated units can also participate in the chelation process. This feature has been exploited to reduce chelated silver to Ag-np via various techniques [26,42,43]. Due to low pH of medium in the present system (pH ≈ 3) it can be anticipated that most amine groups are protonated and therefore Ag^+ has less chance of complexing with them. As the polymer moves toward the negative electrode under the EPD voltage, the high local pH leads to deprotonation of amines and formation of silver–chitosan

Please cite this article in press as: Pishbin F et al. Single-step electrochemical deposition of antimicrobial orthopaedic coatings based on a bioactive glass/chitosan/nano-silver composite system. Acta Biomater (2013), http://dx.doi.org/10.1016/j.actbio.2013.03.006

complexes. Consequently, the availability of electrons at the negative electrode results in reduction of silver ions to Ag-np. In this context, chitosan acts as a controller of Ag-np nucleation and protects these nanoparticles from agglomeration. Indeed, TEM images show (Fig. 5a and b) that Ag-np were deposited adjacent to the electrode surface. In this context, gelation of chitosan as an electrically insulating layer on the Ag-np layer can prevent further formation of Ag-np.

In CS/BG/Ag EPD, a similar mechanism is active. Comparisons of FTIR spectra obtained from CS/BG/Ag and CS films (Fig. 8) and the changes in the intensity of peaks can be related to two phenomena. One is the shift in the Bioglass® Si–O–Si bending vibration which is due to formation of hydrogen bonds between the oxygen of the glass network and hydroxyl groups and amine groups of chitosan [38]. The other phenomenon is the change in the intensity of carbonyl and amine groups of chitosan, in comparison to the peaks in the CS spectrum, which can be due to the formation of a bond between O and N atoms of chitosan molecules and silver ions.

In the CS/BG/Ag system, because a higher voltage (15 V) was used compared to the CS/Ag system (10 V), a thicker layer of Ag-np was deposited. Also, addition of Bioglass® particles to the suspension and their partial dissolution causes an increase in the pH of the suspension (from about pH 3 in CS/Ag solution to pH 4.2 in CS/BG/Ag suspension). At higher pH, fewer chitosan amine groups are protonated and therefore more electron pairs are available to chelate silver ions [44]. This effect, in turn, can lead to formation of more Ag-np nucleation sites and finally smaller-sized Ag-np are deposited. As discussed in the Introduction, the EPD of chitosan/HA film containing silver has been studied previously [31], but deposits were shown to be amorphous and contained ionic silver complexed with chitosan. In this study, it has been demonstrated for the first time that silver can be deposited as nanoparticles using EPD. Here, the formation of Ag-np can be due to the higher suspension pH and the higher EPD voltages applied. The former promotes formation of more silver–chitosan complexes and the latter provides a larger driving force for electroreduction of ionic silver to metallic nanoparticles.

The composite coatings in this study developed a HCAp surface layer after immersion in SBF, which is an indication of bioactivity. The Ca/P atomic ratios of the precipitated phase as measured by EDX are 1.50 ± 0.05 and 1.43 ± 0.03 for CS/BG and CS/BG/Ag, respectively. Bone mineral is a carbonated HAp with a non-stoichiometric Ca/P atomic ratio (1.57–1.62) [45]. The slightly lower Ca/P atomic ratio in this study can be due to the substitution of Mg atoms in the HAp structure and also because the test was performed with the samples not in equilibrium with the CO_2 atmosphere as in physiological conditions. Both of these parameters have been shown to result in formation of a calcium-deficient apatite with lower Ca/P ratios [45,46]. The HAp-forming ability in SBF has been widely assumed to be an indication of bioactivity in vivo and is thought to facilitate formation of a bond between the coated implant and the adjacent bone [33]. However, the SBF test according to Kokubo's recipe (and its corresponding standard as in Ref. [47]) has been critically discussed by Bohner et al. [48] who have pointed out the shortcomings of this method and have proposed improvements for in vitro bioactivity testing. With this in mind, the SBF testing in this research can be considered as a comparative tool to demonstrate the HAp-forming ability of Bioglass®-containing CS/BG and CS/BG/Ag coatings vs. CS coatings based on a standardized method. In this study, two different morphologies of HAp were observed: plate-like on CS/BG/Ag coatings and rod-like particles on CS/BG coatings, which may be related to the high wt.% of chitosan incorporated in CS/BG/Ag determined by TGA. It has been reported that at the SBF pH (7.40), which is above the isoelectric pH of chitosan (6.4), polymer hydroxyl groups acquire negative surface charge [49]:

$$CS - OH + OH^- \rightarrow CS - O^- + H_2O$$

The higher amount of negative surface charge due to the chitosan component in CS/BG/Ag coatings results in more Ca^{2+} absorption on the surface from the SBF solution. Li et al. [50] have attributed plate-like apatite formation to a calcium-dominated frontier at the interface between SBF and the growing HAp layer. The importance of this aspect is related to the different morphologies of HAp found in various biological tissues, e.g. the HAp in bone is plate-like while the one in enamel is rod-like [51].

During immersion in SBF, Ag^+ ions are released into the medium. The initial burst release in the medium can be due to the release of silver from the surface layer of the coating. This is followed by a second stage which varies linearly with the square root of time which implies that the process is controlled by diffusion of silver ions through the coating [52]. Two mechanisms for release of silver ion can be anticipated: (i) degradation of chitosan by erosion and subsequent release of non-reduced silver ions previously complexed with chitosan, and (ii) diffusion of water in the polymer matrix and release of Ag^+ from nanoparticles. Comparison between the release profiles of monolayer and bilayer silver-containing composites indicates the possibility of confining the silver release layer in order to control the release rate. It was shown that less than 7 wt.% of the loaded silver is released within 28 days of SBF treatment. This low concentration of silver ions could efficiently provide bacteriostatic effects on *S. aureus* in vitro. The bactericidal property of silver ions has been associated with the combination of silver ions with the respiratory enzyme or the nucleic acid of bacteria and consequent death of the microorganism. Binding to DNA and proteins of the bacteria is another mechanism suggested for the bactericidal capability of silver ions. On the other hand, Ag-np enhance the antibacterial effect due to penetration inside the bacteria and disruption of its metabolic activity [25]. Although a very low concentration of silver ions was released, a certain cytotoxic effect was observed on MG-63 cells. High concentrations of silver have been reported to be cytotoxic due to a concentration- and time-dependent depletion of intracellular adenosine triphosphate content [53]. Based on the findings of this research, to avoid the cytotoxic effects of silver, it is suggested that a lower concentration of silver be incorporated in the composite structure during electrophoretic deposition.

5. Conclusions

Bioactive and antibacterial composite coatings for potential orthopaedic applications were electrophoretically deposited on metallic substrate. A novel approach was utilized for *in situ* formation and single-step deposition of Ag-np in a multifunctional chitosan/bioactive glass coating. The coatings demonstrated uniform formation of Ag-np and were bioactive in terms of HAp formation in SBF. The sustained release of silver ions from the coatings facilitated bactericidal activity in vitro. Although the levels of incorporated silver in composite coatings under study demonstrated cytotoxic effects on osteoblast-like cells, this preliminary investigation paves the way for improvement of such multifunctional structures. One important feature of the developed method is *in situ* formation and encapsulation of Ag-np, which avoids possible environmental hazards associated with loose nanoparticles. Future work consists of exploring the suitable range of Ag-np loading which provides a minimum inhibitory concentration against bacteria as well as supporting cellular attachment and proliferation. Further work also involves investigating the potential of EPD in tuning the silver release kinetics through sequential deposition of different layers and/or modification of deposition parameters. Additionally, evaluation of the interfacial bonding of these coatings to the substrate and the mechanical properties of the developed films need to be addressed before clinical applications can be considered.

Please cite this article in press as: Pishbin F et al. Single-step electrochemical deposition of antimicrobial orthopaedic coatings based on a bioactive glass/chitosan/nano-silver composite system. Acta Biomater (2013), http://dx.doi.org/10.1016/j.actbio.2013.03.006

Acknowledgments

F. P. would like to thank Imperial College London for granting a scholarship under Overseas Research Students Awards Scheme (ORSAS). She also wishes to thank Mr. Mohamed H. Parkar (Eastman Dental Institute, UCL, London, UK) for providing training on cellular experiments and Mr. Richard Sweeney (Imperial College London, UK) for assistance in TGA tests. The authors are grateful to Dr. I. Thompson (Kings College London, UK) for supplying the Bioglass® powder.

Appendix A. Figures with essential colour discrimination

Certain figures in this article, particularly Figs. 3, 4, 7, 8, 9 and 10 are difficult to interpret in black and white. The full colour images can be found in the on-line version, at http://dx.doi.org/10.1016/j.actbio.2013.03.006.

References

[1] Geetha M, Singh AK, Asokamani R, Gogia AK. Ti based biomaterials, the ultimate choice for orthopaedic implants—a review. Prog Mater Sci 2009;54:397–425.
[2] Lansdown AB. Silver. I: Its antibacterial properties and mechanism of action. J Wound Care 2002;11:125–30.
[3] Hench LL, Andersson O. Bioactive glass coatings. In: Hench LL, Wilson J, editors. An introduction to bioceramics. Singapore: World Scientific; 1999. p. 239–59.
[4] Boccaccini A, Peters C, Roether J, Eifler D, Misra S, Minay E. Electrophoretic deposition of polyetheretherketone (PEEK) and PEEK/Bioglass® coatings on NiTi shape memory alloy wires. J Mater Sci 2006;41:8152–9.
[5] Pishbin F, Simchi A, Ryan MP, Boccaccini AR. Electrophoretic deposition of chitosan/45S5 Bioglass (R) composite coatings for orthopaedic applications. Surf Coat Technol 2011;205:5260–8.
[6] Stamboulis A, Hench LL. Bioresorbable polymers: their potential as scaffolds for Bioglass (R) composites. Aedermannsdorf: Trans Tech Publications; 2000. pp. 729–732.
[7] Nijhuis A, Leeuwenburgh S, Jansen J. Wet-chemical deposition of functional coatings for bone implantology. Macromol Biosci 2010;10:1316–29.
[8] Di Martino A, Sittinger M, Risbud MV. Chitosan: a versatile biopolymer for orthopaedic tissue-engineering. Biomaterials 2005;26:5983–90.
[9] Muzzarelli RAA. Chitosan composites with inorganics, morphogenetic proteins and stem cells, for bone regeneration. Carbohydr Polym 2011;83:1433–45.
[10] Simchi A, Pishbin F, Boccaccini AR. Electrophoretic deposition of chitosan. Mater Lett 2009;63:2253–6.
[11] Altomare L, Draghi L, Chiesa R, De Nardo L. Morphology tuning of chitosan films via electrochemical deposition. Mater Lett 2012;78:18–21.
[12] Cheng Y, Luo X, Betz J, Buckhout-White S, Bekdash O, Payne G. In situ quantitative visualization and characterization of chitosan electrodeposition with paired sidewall electrodes. Soft Matter 2010;6:3177–83.
[13] Zhang Z, Jiang T, Ma KN, Cai XJ, Zhou Y, Wang YN. Low temperature electrophoretic deposition of porous chitosan/silk fibroin composite coating for titanium biofunctionalization. J Mater Chem 2011;21:7705–13.
[14] Duan K, Wang R. Surface modifications of bone implants through wet chemistry. J Mater Chem 2006;16:2309–21.
[15] Davies D. Understanding biofilm resistance to antibacterial agents. Nat Rev Drug Discovery 2003;2:114–22.
[16] Popat KC, Eltgroth M, LaTempa TJ, Grimes CA, Desai TA. Titania nanotubes: a novel platform for drug-eluting coatings for medical implants? Small 2007;3:1878–81.
[17] Simchi A, Tamjid E, Pishbin F, Boccaccini AR. Recent progress in inorganic and composite coatings with bactericidal capability for orthopaedic applications. Nanomed Nanotechnol 2011;7:22–39.
[18] Ewald A, Hösel D, Patel S, Grover LM, Barralet JE, Gbureck U. Silver-doped calcium phosphate cements with antimicrobial activity. Acta Biomater 2011;7:4064–70.
[19] Francolini I, D'Ilario L, Guaglianone E, Donelli G, Martinelli A, Piozzi A. Polyurethane anionomers containing metal ions with antimicrobial properties: thermal, mechanical and biological characterization. Acta Biomater 2010;6:3482–90.
[20] Kumar R, Münstedt H. Silver ion release from antimicrobial polyamide/silver composites. Biomaterials 2005;26:2081–8.
[21] Chen Y, Zheng X, Xie Y, Ding C, Ruan H, Fan C. Anti-bacterial and cytotoxic properties of plasma sprayed silver-containing HA coatings. J Mater Sci Mater Med 2008;19:3603–9.
[22] Ling Feng Q, Nam Kim T, Wu J, Seo Park E, Ock Kim J, Young Lim D, et al. Antibacterial effects of Ag-HAp thin films on alumina substrates. Thin Solid Films 1998;335:214–9.
[23] Chen W, Liu Y, Courtney HS, Bettenga M, Agrawal CM, Bumgardner JD, et al. In vitro anti-bacterial and biological properties of magnetron co-sputtered silver-containing hydroxyapatite coating. Biomaterials 2006;27:5512–7.
[24] Chung R-J, Hsieh M-F, Huang C-W, Perng L-H, Wen H-W, Chin T-S. Antimicrobial effects and human gingival biocompatibility of hydroxyapatite sol–gel coatings. J Biomed Mater Res B Appl Biomater 2006;76B:169–78.
[25] Rai M, Yadav A, Gade A. Silver nanoparticles as a new generation of antimicrobials. Biotechnol Adv 2009;27:76–83.
[26] Fu J, Ji J, Fan D, Shen J. Construction of antibacterial multilayer films containing nanosilver via layer-by-layer assembly of heparin and chitosan–silver ions complex. J Biomed Mater Res Part A 2006;79A:665–74.
[27] Sanpo N, Tan M, Cheang P, Khor KA. Antibacterial property of cold-sprayed HA-Ag/PEEK coating. J Therm Spray Technol 2009;18:10–5.
[28] Roy M, Bandyopadhyay A, Bose S. In vitro antimicrobial and biological properties of laser assisted tricalcium phosphate coating on titanium for load bearing implant. Mater Sci Eng C 2009;29:1965–8.
[29] Besra L, Liu M. A review on fundamentals and applications of electrophoretic deposition (EPD). Prog Mater Sci 2007;52:1–561.
[30] Boccaccini AR, Keim S, Ma R, Li Y, Zhitomorsky I. Electrophoretic deposition of biomaterials. J R Soc Interface 2010;7:S581–613.
[31] Pang X, Zhitomirsky I. Electrodeposition of hydroxyapatite–silver–chitosan nanocomposite coatings. Surf Coat Technol 2008;202:3815–21.
[32] Pishbin F, Simchi A, Ryan MP, Boccaccini AR. A study of the electrophoretic deposition of Bioglass® suspensions using the Taguchi experimental design approach. J Eur Ceram Soc 2010;30:2963–70.
[33] Kokubo T, Takadama H. How useful is SBF in predicting in vivo bone bioactivity? Biomaterials 2006;27:2907–15.
[34] Hench LL. Repair of skeletal tissues. In: Hench LL, Jones JR, editors. Biomaterials, artificial organs and tissue engineering. Cambridge: Woodhead Publishing; 2005. p. 119–28.
[35] Langford RM, Clinton C. In situ lift-out using a FIB-SEM system. Micron 2004;35:607–11.
[36] Pang X, Zhitomirsky I. Electrodeposition of composite hydroxyapatite–chitosan films. Mater Chem Phys 2005;94:245–51.
[37] Zhitomirsky D, Roether JA, Boccaccini AR, Zhitomirsky I. Electrophoretic deposition of bioactive glass/polymer composite coatings with and without HA nanoparticle inclusions for biomedical applications. J Mater Process Technol 2009;209:1853–60.
[38] Paluszkiewicz C, Stodolak E, Hasik M, Blazewicz M. FT-IR study of montmorillonite–chitosan nanocomposite materials. Spectrochim Acta Part A Mol Biomol Spectrosc 2011;79:784–8.
[39] Kontonasaki E, Zorba T, Papadopoulou L, Pavlidou E, Chatzistavrou X, Paraskevopoulos K, et al. Hydroxy carbonate apatite formation on particulate bioglass in vitro as a function of time. Cryst Res Technol 2002;37:1165–71.
[40] Mourino V, Newby P, Pishbin F, Cattalini JP, Lucangioli S, Boccaccini AR. Physicochemical, biological and drug-release properties of gallium crosslinked alginate/nanoparticulate bioactive glass composite films. Soft Matter 2011;7:6705–12.
[41] Huang H, Yuan Q, Yang X. Preparation and characterization of metal–chitosan nanocomposites. Colloids Surf B 2004;39:31–7.
[42] Chen P, Song L, Liu Y, Fang Y-e. Synthesis of silver nanoparticles by γ-ray irradiation in acetic water solution containing chitosan. Radiat Phys Chem 2007;76:1165–8.
[43] Huang H, Yang X. Synthesis of polysaccharide-stabilized gold and silver nanoparticles: a green method. Carbohydr Res 2004;339:2627–31.
[44] Lasko CL, Hurst MP. An investigation into the use of chitosan for the removal of soluble silver from industrial wastewater. Environ Sci Technol 1999;33:3622–6.
[45] Kim HM, Kishimoto K, Miyaji F, Kokubo T, Yao T, Suetsugu Y, et al. Composition and structure of apatite formed on organic polymer in simulated body fluid with a high content of carbonate ion. J Mater Sci Mater M 2000;11:421–6.
[46] BarrÈre F, Layrolle P, van Blitterswijk CA, de Groot K. Biomimetic calcium phosphate coatings on Ti6Al4V: a crystal growth study of octacalcium phosphate and inhibition by Mg^{2+} and HCO^{3-}. Bone 1999;25:107S–11S.
[47] ISO 23317:2012; Implants for surgery. In vitro evaluation for apatite-forming ability of implant materials, International Organization for Standardization, Geneva, Switzerland.
[48] Bohner M, Lemaitre J. Can bioactivity be tested in vitro with SBF solution? Biomaterials 2009;30:2175–9.
[49] Sharma S, Soni V, Bellare J. Chitosan reinforced apatite–wollastonite coating by electrophoretic deposition on titanium implants. J Mater Sci Mater Med 2009;20:1427–36.
[50] Li P, Nakanishi K, Kokubo T, de Groot K. Induction and morphology of hydroxyapatite, precipitated from metastable simulated body fluids on sol-gel prepared silica. Biomaterials 1993;14:963–8.
[51] H-b Zhang, K-c Zhou, Z-y Li, S-p Huang. Plate-like hydroxyapatite nanoparticles synthesized by the hydrothermal method. J Phys Chem Solids 2009;70:243–8.
[52] Yu H, Xu X, Chen X, Lu T, Zhang P, Jing X. Preparation and antibacterial effects of PVA-PVP hydrogels containing silver nanoparticles. J Appl Polym Sci 2007;103:125–33.
[53] Hidalgo E, Dominguez C. Study of cytotoxicity mechanisms of silver nitrate in human dermal fibroblasts. Toxicol Lett 1998;98:169–79.